Supplementary Material

1. Forward model *tT* inputs

1.1 Mount Timpanogos

Sample 10UTT7 from the Mount Timpanogos transect was collected in the Bridal Veil Limestone member of the Oquirrh Group, while 10UTT6 was collected in the Bear Canyon Formation of the Oquirrh Group. The Bridal Veil Limestone member is Morrowan in age (312 Ma, Maxfield, 1957) with an estimated 6320 m of additional Oquirrh group strata overlying it in the vicinity of Mount Timpanogos (Larson and Clark, 1979; Konopka and Dott, 1982; Hintze and Kowallis, 2009). These units include the Bear Canyon Formation, Shingle Mill Limestone, Wallsburg Ridge Formation, and Granger Mountain Formation and range in age from Atokan (312 Ma) to Wolfcampian (280 Ma). Above the Oquirrh Group, composite stratigraphic charts for this area document 1050 m of Permian Kirkman Limestone through Park City Group (Hintze and Kowallis, 2009).

Mesozoic rocks are absent from this location and we estimate their missing thicknesses. Due to our transect's relative proximity to Salt Lake City, we use Solien's (1979) 700 m of Thaynes Formation for the thickness of Lower Triassic rocks at Mount Timpanogos. The Upper Triassic-Lower Jurassic section is completely absent throughout much of western Utah and the total extent and thicknesses of the Chinle Formation and Glen Canyon Group in this area—the units that overlie the Thaynes in other parts of Utah—are speculative. Hintze and Davis (2003) reported 230 m of Chinle Formation in the Pahvant Range, which represents some of the westernmost exposures of this unit. These authors also described well-logs near Sevier Lake in western Utah that contained 450 m of Lower Jurassic Navajo Sandstone. Restoration along the Sevier Desert

Detachment placed this well against the western flank of the Pahvant Range (DeCelles and Coogan, 2006), which is still some distance away from our transect. Regardless, these thicknesses represent perhaps the best estimate of missing equivalent strata at Mount Timpanogos. add our conjectural Chinle-Navajo thicknesses to complete the Upper Triassic-Lower Jurassic sequence. To the north and south of Mount Timpanogos, Imlay (1967) measured 390 m and 880 m of Twin Creek Limestone-Arapien Shale at Thistle and Salt Lake City, respectively. We average these two numbers together and use 635 m as a representative thickness for Middle Jurassic (160 Ma) rocks deposited on top of our transect. Finally, we estimate that roughly 1000 m of additional Early Cretaceous foredeep units were deposited above Mount Timpanogos prior to exhumation (DeCelles, 2004).

1.2 Oquirrh Mountains

All samples in the Oquirrh Mountains transect were collected in the Butterfield Peaks Formation of the Oquirrh Group. The Butterfield Peak Formation has a total thickness of 2770 m (Tooker and Roberts, 1970; Clark et al., 2012), and we estimate that our transect sits in the middle with approximately 1390 m of additional Butterfield Peak overlying it. Above this formation are the Moscovian Bingham Mine Formation (1980 m, Hintze and Kowallis, 2009) and the Wolfcampian Oquirrh units: the Freeman Peak Formation, Curry Peak Formation, and the Kirkman Limestone (1550 m). Bissell (1959) also described rocks of the Diamond Creek Sandstone and the lower Park City Group in the Oquirrh Mountains, which are Leonardian in age (~270 Ma) and 760 m thick. This brings the total thickness of the Pennsylvanian-Permian stratigraphy in the Oquirrh Mountains to 5680 m.

The next youngest units that crop out in the Oquirrh Mountains are Oligocene age volcanic and igneous units (Moore, 1973). Like the Stansbury Mountains, Mesozoic strata are completely absent from this range, but we assume that units similar in age and thickness to those used in our Stansbury *tT* paths were also deposited on top of our Oquirrh transect. These include the Thaynes Limestone and our conjectural Chinle through Navajo sequence. The Thaynes Limestone crops out both to the west of our Oquirrh transect in the Stansbury Range and also to the east, in the vicinity of Salt Lake City, where it is more than twice as thick—700 m as opposed to 340 m (Solien, 1979). We use the same thickness for Thaynes deposition in the Oquirrh Mountains as in the Stansbury Mountains, but note that this unit could have been thicker. Finally, we include 1000 m of Early Cretaceous (140-110 Ma) foredeep strata (DeCelles, 2004) in our model thermal histories.

1.3 Stansbury Mountains

Mapping relationships and cross-sections (fig. 4 in main text) show that our Stansbury transect samples come from the upper part of the lower Cambrian Prospect Mountain Formation. Initial deposition is therefore placed at 521 Ma with another ~400 m of Prospect Mountain Formation overlying our samples. For the remaining Cambrian through upper Mississippian sedimentary thicknesses, we use the measured sections and maps of Rigby (1958), Hintze and Kowallis (2009), and Clark et al. (2012). Where disagreements about unit nomenclature exist, we rely upon the most recent description of the given unit. Above the Prospect Mountain Formation, an additional 670 m of Cambrian sediments (Pioche through Orr Formations) were conformably deposited at our location (fig. 4). The next overlying units are of latest Devonian and earliest

Mississippian and consist of the Stansbury Formation, Pinyon Peak Limestone, Fitchville Formation, and Gardison Limestone (370 m total). In the Stansbury Range, these units are an eastern expression of the Late Devonian Antler Orogeny (Rigby, 1958; Silberling et al., 1997), and were either deposited during deformation (Stansbury Formation) or immediately after deformation (Pinyon Peak Limestone, Fitchville Formation, Gardison Limestone). In our HeFTy models, we represent exhumation related to the Antler Orogeny as a period of rapid cooling in the Late Devonian. For the thicknesses of the missing units (uppermost Cambrian Ajax Dolomite through Early Devonian Simonson Dolomite), we rely upon the Stansbury Range composite stratigraphic chart of Hintze and Kowallis (2009) that gives a total missing thickness of 1020 m. The end of Simonson Dolomite deposition brackets the beginning of this exhumation event and is thought to be early Givetian in age (~390 Ma, Sandberg et al., 1982). The upper bound on this event is marked by deposition of the middle Famennian (~370 Ma) Pinyon Peak Limestone (Sandberg and Gutschick, 1979). Another 1230 m of conformable Mississippian strata from the Deseret Formation to the Manning Canyon Shale overlies the Gardison Limestone.

The next major phase of sedimentary burial is represented by the thick succession of Early Pennsylvanian through early Permian rocks of the Oquirrh Group. In the Stansbury Range, the beginning of Oquirrh Group deposition is marked by the Butterfield Peaks Formation, which is 1800 m thick and Moscovian in age (Armin and Moore, 1981; Stevens and Armin, 1983). An additional 3500 m of Oquirrh Group strata consisting of the Bingham Mine, Freeman Peak, and Curry Peak Formations, were deposited on top of the Butterfield Peaks Formation. Oquirrh Group deposition ended during the late

Wolfcampian (Jordan, 1979; Hintze and Kowallis, 2009). This brings the total Oquirrh Group thickness to 5300 m.

The final phase of sedimentary burial occurred from the late Permian until the Late Cretaceous and is the most enigmatic in terms of the units deposited and their thicknesses. Jordan and Allmendinger (1979) described 780 m of lower Permian (~280 Ma) Kirkman Limestone through Lower Triassic (~245 Ma) Thaynes Limestone exposed in the Martin Fork syncline of the eastern Stansbury Mountains. To this, we add our conjectural Chinle-Navajo thicknesses (see previous sections) to complete the Triassic-Lower Jurassic sequence. Regional isopachs suggest at least an additional 1000 m of Early to middle Cretaceous (140-110 Ma) foredeep strata were deposited over our transect (DeCelles, 2004) and we include these numbers in all models.

2. Zonation effects

2.1 Zonation model inputs

Models were constructed for each dataset to assess the degree to which zonation might influence our *tT* interpretations. This assessment is limited by the fact that we did not collect zonation measurements on individual grains, as is typical for most conventional zircon He dating studies. As such, our aim is simply to provide a sense of the degree to which model date-eU curves constructed with a particular style of zonation might differ from our assumed, unzoned model curves. We show date-eU curves that have either systematically eU-enriched cores (high eU cores) or systematically eU-enriched rims (high eU rims) for different zonation styles. The styles of zonation depict both moderate degrees of zonation, with a factor of two enrichment (by a step-function) in a model grain's core or rim eU concentration (referred to as 2x curves in the accompanying figures), and more extreme degrees of zonation, with order of magnitude enrichment in a model grain's core or rim eU concentration (referred to as 10x in the accompanying figures). Each curve is then compared to an unzoned curve, which has model grains with equivalent bulk eU concentrations to the high eU core and high eU rim grains in each scenario, but homogenously distributed.

Several variables have to be considered for each model. The radial position of the core and rim in each scenario is an important choice as the effects of zonation on a grain's He concentration profile, alpha ejection correction, and radiation damage-diffusivity profile can become exacerbated at particular positions. Guenthner et al. (2013) described a "zonation impact factor" and found that, for grains with an ~60 μm equivalent spherical radius, zonation has its strongest effects on date-eU relationships when either high eU cores occupy the inner third of the grain, or high eU rims occupy the outer third of the grain. As such, we designate the inner third of the grain as the core in our high eU core curves, and the outer third as the rim in our high eU rim curves. We use the mean equivalent spherical radii of each dataset (54 μm for the Stansbury transect, 43 μm for the Oquirrh transect, and 40 μm for Timpanogos), but we also plot the two standard deviations grain size date-eU curves for the unzoned grains in order to compare the possible degree of dispersion caused by grain size differences with dispersion caused by zonation. Finally, a choice of alpha ejection correction is needed: either the "correct" correction that accounts for redistribution of He inside the grain, or the "naïve" correction, which is a correction applied to a zoned grain assuming an homogenous distribution of U and Th. Because we are primarily interested in the discrepancies that result from a false assumption of homogeneity, we use the naïve correction in all models.

2.2 Zonation model results

The results from our zonation modeling are presented in figures DR1-3. Due to the nature of the damage-diffusivity relationship (decrease and subsequent increase in diffusivity with progressive damage accumulation), we expect that zoned grains can possess distinct domains with highly variable diffusivities, which can lead to complex behavior for a specific *tT* history. Still, we can provide some general observations, applicable to all three datasets, drawn from our results. At low bulk eU concentrations, the high eU core grains are nearly identically to their unzoned counterparts, but become slightly younger (by ~10-20 Ma) at high bulk eU concentrations. We attribute the behavior at low bulk eU to the contrasting diffusivities between rim and core. Despite a potentially high damage (and therefore high diffusivity) core, the rim acts as a lower diffusivity rind or “shield” that balances out the higher diffusivity core such that the bulk diffusivity is roughly similar to the unzoned grain. At high bulk eU concentrations, the rim likely becomes damaged enough that it no longer acts as a shield and instead contributes to bulk diffusivities that are higher than unzoned grains (hence, giving younger dates).

For the high eU rim zircon, nearly all of the date-eU curves are shifted to younger dates when compared to their unzoned equivalents. These younger dates likely result from our (purposeful) use of the naïve alpha ejection correction, whereby the correction is insufficient at accounting for the He lost to alpha ejection (i.e. more He was lost from the rim due to ejection than is assumed). The effect of damage on diffusivity also plays a role though, particularly at high bulk eU concentrations where rims with high diffusivities are expected to lead to greater He loss than the unzoned grains and therefore younger dates.

3. Maximum burial temperatures for the Oquirrh transect

In order to further constrain the maximum burial temperature for the Oquirrh transect, we used sample 10UTOO10—500 m stratigraphically below the rest of the Oquirrh samples—as an additional cross-check. We first constructed a *tT* path using the same geothermal gradient (20 °C/km), timing of exhumation (110 Ma), and magnitude of exhumation (3 km) from the preferred exhumation scenario for the entire Oquirrh dataset, but increased the burial depth (specifically the thickness of the Oquirrh Group) by 500 m. With this revised *tT* path, we then generated an inheritance envelope and compared it to the dates from sample 10UTOO10 only (triangles in fig. DR6). If this revised inheritance envelope explains the 10UTOO10 dates, then our maximum burial temperature for the rest of the dataset (constrained from the same inputs, just 500 m less burial depth) is valid. As figure DR6 shows, a 20 °C/km geothermal gradient generates an acceptable inheritance envelope for the main portion of the Oquirrh transect (maximum burial temperature of 173 °C), but not sample 10UTOO10 (maximum burial temperature of 183 °C). However, a *tT* path constructed from a lower geothermal gradient of 19 °C/km (but the same timing and magnitude of exhumation) gives inheritance envelopes that explain the observed dispersion in both the main portion of the Oquirrh transect, and sample 10UTOO10. This lower geotherm gives a maximum burial temperature for the main Oquirrh transect of 166 °C.

4. Additional references not in the main text

Armin, R.A., and Moore, W.J., 1981, Geology of the southeastern Stansbury Mountains and southern Onaqui Mountains, Tooele County, Utah: U.S. Geological Survey Open-File Report 81-0247.

Bissell, H.J., 1959, Stratigraphy of the southern Oquirrh Mountains, Pennsylvanian system: Utah Geological Society Guidebook, v. 14, p. 93-127.

DeCelles, P.G., and Coogan, J.C., 2006, Regional structure and kinematic history of the Sevier fold-and-thrust belt, central Utah: Geological Society of America Bulletin, v. 118, p. 841-864.

Hintze, L.F., and Davis, F.D., 2003, Geology of Millard County, Utah: Utah Geological Survey Bulletin, v. 133, 305 p.

Imlay, R.W., 1967, Twin Creek Limestone (Jurassic) in the western interior of the United State: U.S. Geological Survey Professional Paper 540, 105p.

Jordan, T.E., 1979, Evolution of the late Pennsylvanian-early Permian western Oquirrh Basin, Utah: Ph.D. thesis, Stanford University, Palo Alto, 253 p.

Jordan, T.E., and Allmendinger, R.W., 1979, Upper Permian and Lower Triassic stratigraphy of the Stansbury Mountains, Utah: Utah Geology, v. 6, p. 69-74.

Konopka, E.H., and Dott, R.H. Jr., 1982, Stratigraphy and sedimentology, lower part of the Butterfield Peaks Formation (middle Pennsylvanian), Oquirrh Group at Mt. Timpanogos, Utah: Utah Geological Association Publication 10, p. 215-234.

Larson, J.A., and Clark, D.L., 1979, Lower Permian (Sakmarian) portion of the Oquirrh Formation, Utah: Brigham Young University Geology Studies, v. 26, part 3, p. 135-142.

Maxfield, E.B., 1957, Sedimentation and stratigraphy of the Morrowan Series in central Utah: Brigham Young University Geology Studies, v. 4, no. 1, 46 p.

Moore, W.J., 1973, Summary of radiometric ages of igneous rocks in the Oquirrh Mountains, north-central Utah: Economic Geology, v. 68, p. 97-101.

Sandberg, C.A., and Gutschick, R.C., 1979, Guide to conodont biostratigraphy of Osagean and Meramecian starved basin and foreslope, western United States: Rocky Mountain Section, Society of Economic Geologists and Paleontologists, Symposium 1, Paleozoic Paleogeography of west-central United States, p. 129-148.

Sandberg, C.A., Gutschick, R.C., Johnson, J.G., Poole, F.G., and Sando, W.J., 1982, Middle Devonian to Late Mississippian geologic history of the Overthrust Belt region, western U.S.: Rocky Mountain Association of Geologists, Geologic Studies of the Cordilleran Thrust Belt, v. 2, p. 691-719.

Silberling, N.J., Nichols, K.M., Trexler, J.H. Jr., Jewell, P.W., and Crosbie, R.A., 1997, Overview of Mississippian depositional and paleotectonic history of the Antler foreland, eastern Nevada and western Utah, *in* Link, P.K., and Kowallis, B.J., editors, Mesozoic to Recent geology of Utah: Brigham Young University Geology Studies, v. 42, part 2, p. 161-198.

Stevens, C.H., and Armin, R.A., 1983, Microfacies of the Middle Pennsylvanian part of the Oquirrh Group, central Utah, *in* Miller, D.M., Todd, V.R., and Howard, K.A., editors, Tectonic and stratigraphic studies in the eastern Great Basin: Geological Society of America Memoir 157, p. 83-100.

Solien, M.A., 1979, Conodont biostratigraphy of the Lower Triassic Thaynes Formation, Utah: Journal of Paleontology, v. 53, p. 276-306.

Tooker, E.W., and Roberts, R.J., 1970, Upper Paleozoic rocks in the Oquirrh Mountains and Bingham mining district, Utah: U.S. Geological Survey Professional Paper 629-A, 76 p.

Figure Captions

Figure DR1: Forward model results for sample 10UTT7 from the Mount Timpanogos transect using our preferred exhumation scenario (5 km of exhumation at 100 Ma) that include various styles of zonation. Two different styles of zonation are presented: grains with either cores or rims enriched by a factor of two (2x), and grains with cores or rims enriched by an order of magnitude (10x). At any given point along the x axis, individual modeled grains composing each curve contain equivalent bulk eU concentrations. The solid black curve represents the date-eU correlation for unzoned grains with radii of 40 μm (mean), while the dashed grey lines correspond to the 2 sigma standard deviation in grain size (30 and 50 μm), also unzoned. Solid red date-eU curves represent the model trends for the eU-enriched core grains with radii of 40 μm (high eU core) and solid blue date-eU curves represent the model trends for the eU-enriched rim grains with radii of 40 μm (high eU rim). Only the zero-inheritance trends are shown in this figure.

Figure DR2: Forward model results for the Oquirrh transect using our preferred exhumation scenario (3 km of exhumation at 110 Ma) that include various styles of zonation. Presented zonation styles are similar to figure DR2. Solid black curves represent zero-inheritance, unzoned model grains with radii of 43 μm (mean). Black curves with a dash and a dot represent the 1100 Ma unzoned inheritance curve, while dotted black curves represent the 1700 Ma unzoned inheritance curve. All dashed grey curves are for unzoned grain sizes of 61 and 25 μm (2 standard deviations). Red curves represent high eU core grains with radii of 43 μm and the style (i.e. solid, dotted, dash-dot) corresponds with the particular amount of inheritance. Blue curves represent high eU rim grains with radii of 43 μm and the style similarly corresponds with the particular amount of inheritance.

Figure DR3: Forward model results for the Stansbury Mountains transect using our preferred exhumation scenario (5 km of exhumation at 120 Ma) that include various styles of zonation. Presented zonation styles are similar to figure DR2. Solid black curves represent zero-inheritance, unzoned model grains with radii of 54 μm (mean). Black curves with a dash and a dot represent the 1100 Ma unzoned inheritance curve, while dotted black curves represent the 1700 Ma unzoned inheritance curve. All dashed grey curves are for unzoned grain sizes of 75 and 33 μm (2 standard deviations). Red curves represent high eU core grains with radii of 54 μm and the style (i.e. solid, dotted, dash-dot) corresponds with the particular amount of inheritance. Blue curves represent high eU rim grains with radii of 54 μm and the style similarly corresponds with the particular amount of inheritance.

Figure DR4: Additional time-temperature (*tT*) paths and corresponding date-eU plots testing the relative importance of specific points in the forward model inputs for the Mount Timpanogos dataset. This figure compliments figure 10 in the main text and examines the relative importance of a complex versus simplified *tT* path (see main text for details). The style or shading in the *tT* paths on the bottom plot match the style or shading of model date-eU trends on the top plot. The dashed grey lines for each date-eU trend correspond to the 2 sigma standard deviation in grain size (30 and 50 microns, see text).

Figure DR5: Forward model results for sample 10UTT7 from the Mount Timpanogos transect using a *tT* scenario with 5 km of exhumation at 100 Ma, and a geothermal gradient of either 20 °C/km (solid black curves in date-eU and *tT* plot) or 25 °C/km (dotted black curves in date-eU and *tT* plot). Black curves are for grains with radii of 40 μm (mean), while the dashed grey lines correspond to the 2 sigma standard deviation in grain size (30 and 50 μm).

Figure DR6: Forward model results for the main Oquirrh transect, or all samples except 10UTOO10 (circles), and sample 10UTOO10 (triangles) using geothermal gradients of 20 °C/km (top two panels) and 19 °C/km (bottom two panels). In all panels, inheritance envelopes were constructed using *tT* paths from our preferred exhumation scenario for the Oquirrh transect (3 km of exhumation at 110 Ma). The *tT* paths for the 10UTOO10 panels though contain 500 m of additional Oquirrh Group thickness. Listed maximum burial temperatures are the maximum temperatures reached in each *tT* path just prior to initial exhumation at 110 Ma. Black curves are for a grain size of 43 microns (mean), and the dashed grey curves are for grain sizes of 61 and 25 microns (2 standard deviations). Solid black curve is the zero-inheritance curve, the dashed-dot line is the 1100 Ma inheritance curve, and the dotted line is the 1700 Ma inheritance curve.

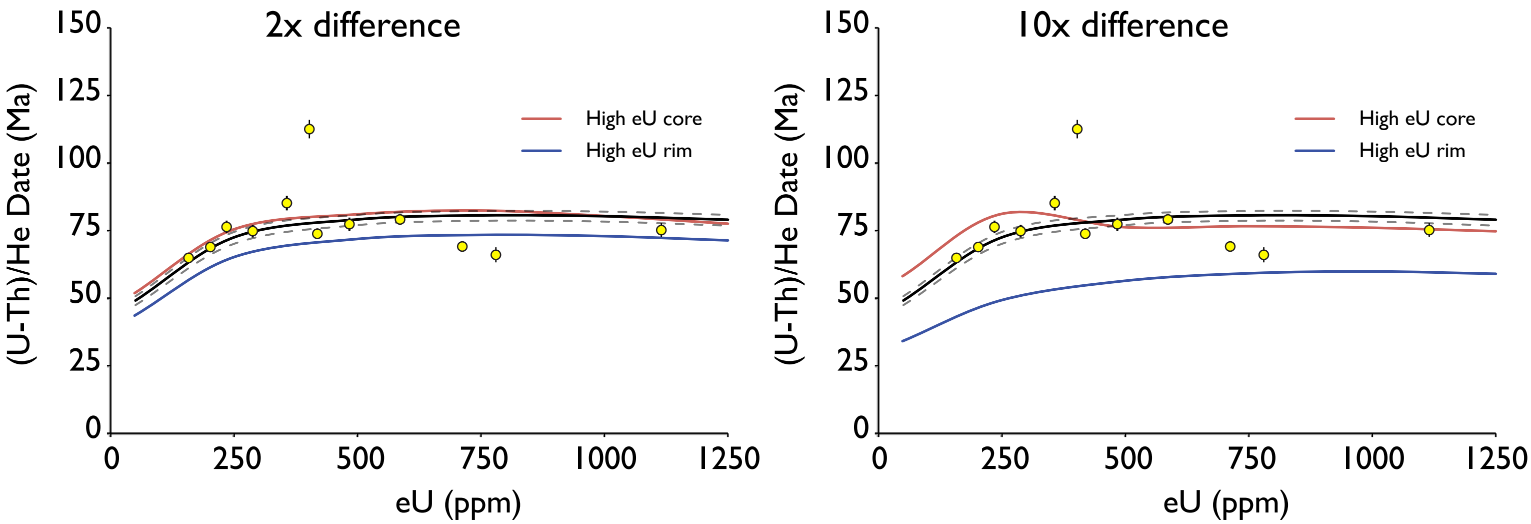
2x difference
10x difference
High eU core
High eU rim
(U-Th)/He Date (Ma)
eU (ppm)
0
25
50
75
100
125
150
250
500
750
1000
1250

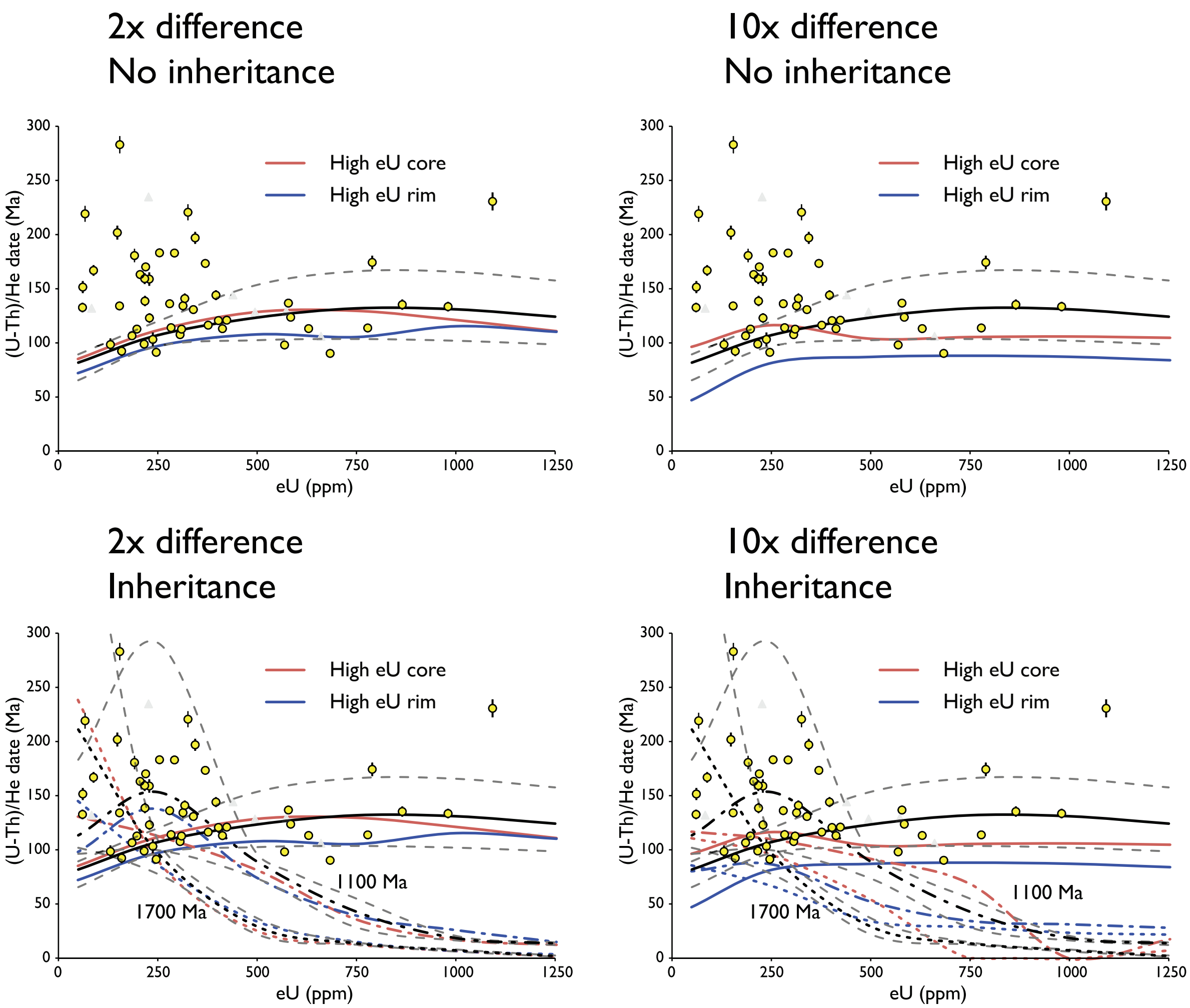
2x difference
No inheritance
High eU core
High eU rim
(U-Th)/He date (Ma)
eU (ppm)
10x difference
No inheritance
High eU core
High eU rim
(U-Th)/He date (Ma)
eU (ppm)
2x difference
Inheritance
High eU core
High eU rim
1100 Ma
1700 Ma
(U-Th)/He date (Ma)
eU (ppm)
10x difference
Inheritance
High eU core
High eU rim
1100 Ma
1700 Ma
(U-Th)/He date (Ma)
eU (ppm)

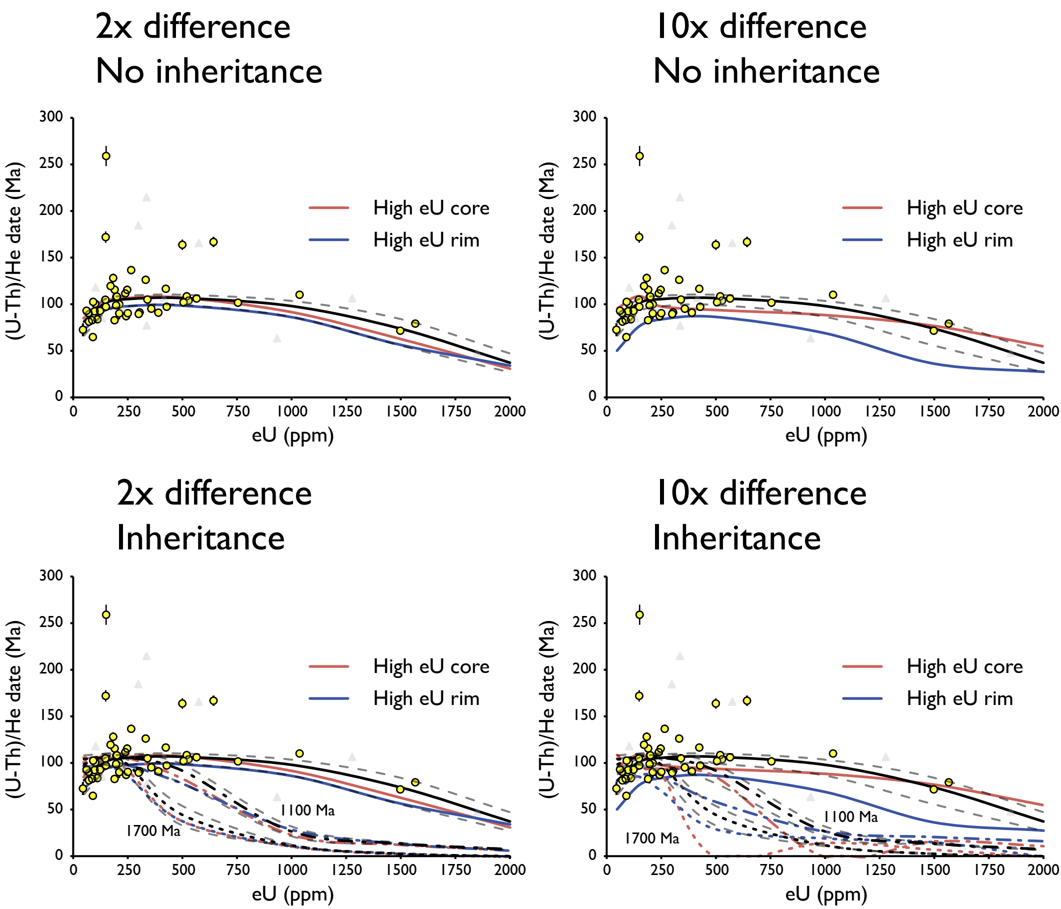
2x difference
No inheritance
10x difference
No inheritance
2x difference
Inheritance
10x difference
Inheritance
(U-Th)/He date (Ma)
eU (ppm)
High eU core
High eU rim
0
50
100
150
200
250
300
0
250
500
750
1000
1250
1500
1750
2000
1100 Ma
1700 Ma

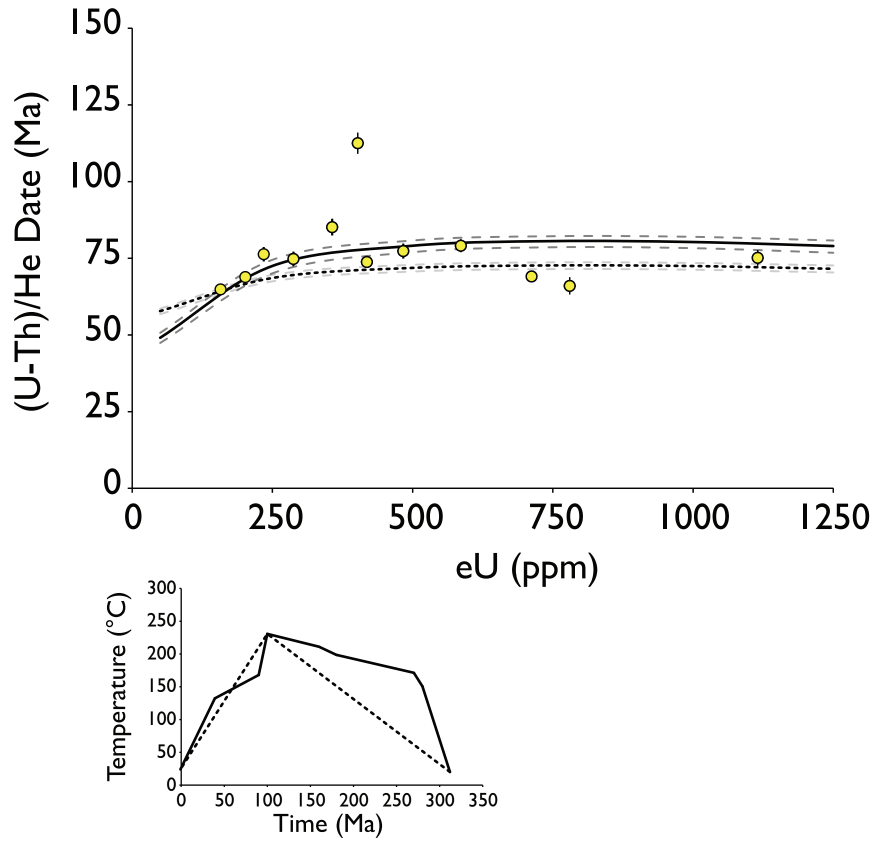

150
125
100
75
50
25
0
(U-Th)/He Date (Ma)
0
250
500
750
1000
1250
eU (ppm)
300
250
200
150
100
50
0
Temperature (°C)
0
50
100
150
200
250
300
350
Time (Ma)

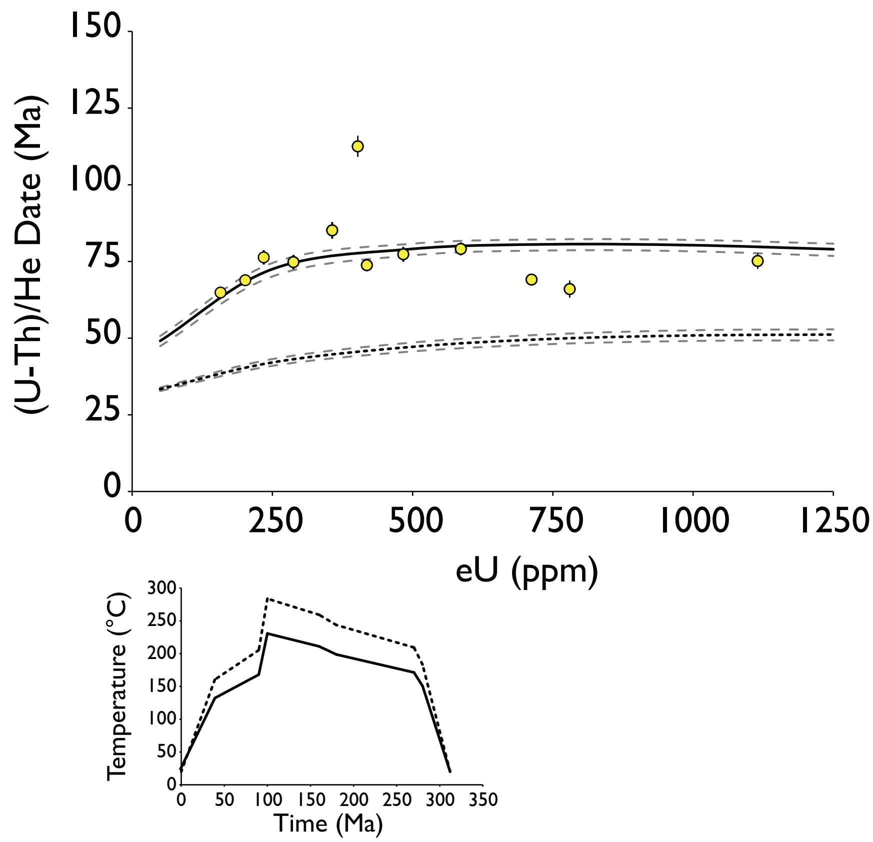
(U-Th)/He Date (Ma)
150
125
100
75
50
25
0
0
250
500
750
1000
1250
eU (ppm)
Temperature (°C)
300
250
200
150
100
50
0
0
50
100
150
200
250
300
350
Time (Ma)

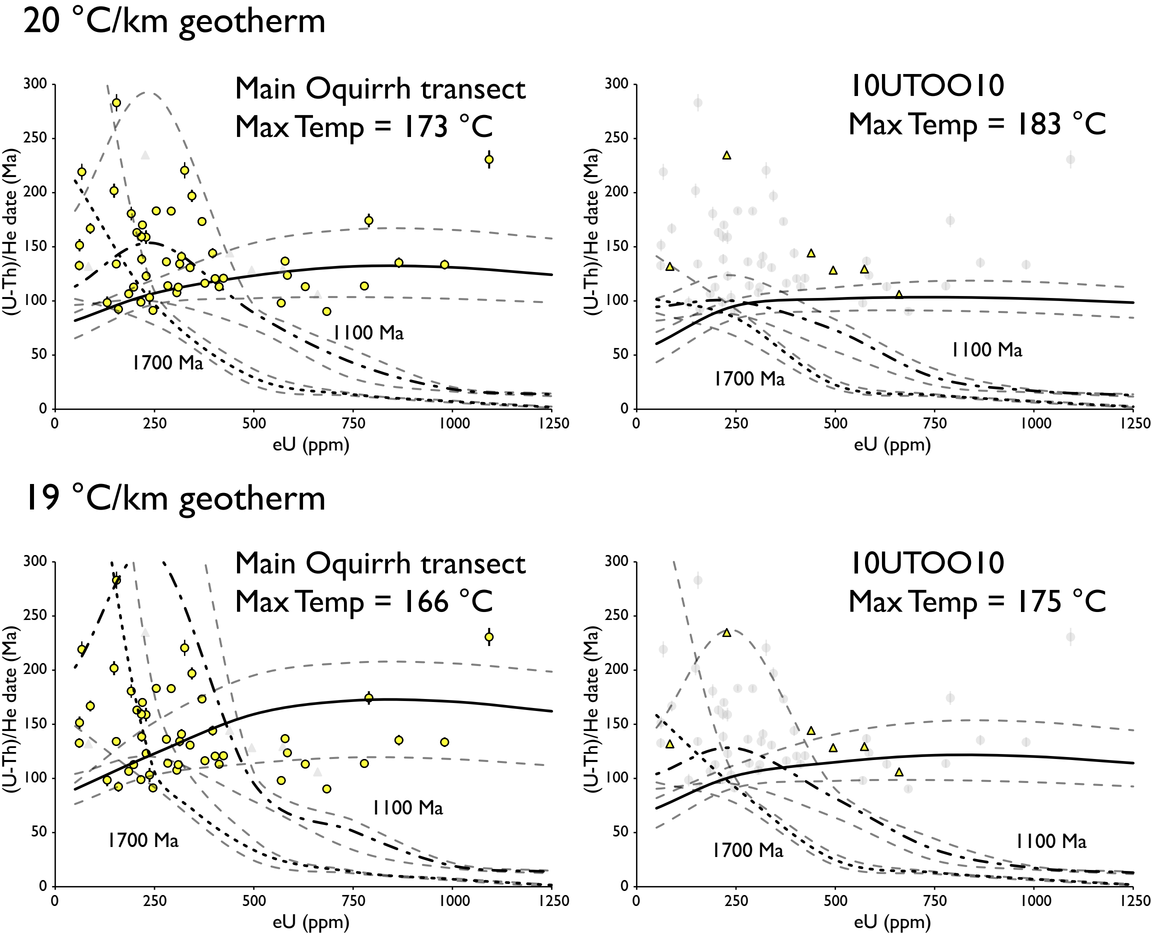
20 °C/km geotherm
Main Oquirrh transect
Max Temp = 173 °C
1100 Ma
1700 Ma
10UTOO10
Max Temp = 183 °C
1100 Ma
1700 Ma
19 °C/km geotherm
Main Oquirrh transect
Max Temp = 166 °C
1100 Ma
1700 Ma
10UTOO10
Max Temp = 175 °C
1100 Ma
1700 Ma
(U-Th)/He date (Ma)
eU (ppm)
0
50
100
150
200
250
300
0
250
500
750
1000
1250